ASTRONOMY & ASTROPHYSICS
SUPPLEMENT SERIES

Astron. Astrophys. Suppl. Ser. **131**, 451–467 (1998)

50 μas resolution VLBI images of AGN's at $\lambda 3$ mm

F.T. Rantakyrö[1,2,⋆], L.B. Bååth[3], D.C. Backer[4], R.S. Booth[5], J.E. Carlstrom[6], D.T. Emerson[7], M. Grewing[8], H. Hirabayashi[9], M.W. Hodges[6], M. Inoue[9], H. Kobayashi[9], T.P. Krichbaum[10], A.J. Kus[11], J.M. Moran[12], M. Morimoto[9], S. Padin[6], R.L. Plambeck[4], R. Predmore[13], A.E.E. Rogers[14], C. Schalinski[8], A. Witzel[10], D. Woody[6], M.C.H. Wright[4], and A. Zensus[15]

[1] Istituto di RadioAstronomia–CNR, Via Gobetti 101, I-40129, Bologna, Italy
[2] Joint Institute for VLBI in Europe, Postbus 2, 7990AA Dwingeloo, The Netherlands
[3] Center for Imaging Technologies, Halmstad University, S-301 18 Halmstad, Sweden
[4] University of California, Berkeley CA 94720, U.S.A.
[5] Onsala Space Observatory, S-439 92 Onsala, Sweden
[6] Owens Valley Observatory, California Institute of Technology, Pasadena CA 91125, U.S.A.
[7] NRAO, 949 N. Cherry Ave., Campus Bldg. 65, Tucson AZ 85721-0655, U.S.A.
[8] IRAM, 300 rue de la Piscine, F-38406 St. Martin d'Hères, France
[9] Nobeyama Radio Observatory, Nobeyama, Minamisaku, Nagano 384-13, Japan
[10] Max-Planck-Institut für Radioastronomie, Auf dem Huegel 69, D-53121 Bonn, Germany
[11] Torun Radio Observatory, Nicolau Copernicus Observatory, Torun, Poland
[12] Center for Astrophysics, 60 Garden Street, Cambridge MA 02138, U.S.A.
[13] FCRAO, Dept. of Physics and Astronomy, 619 Lederle Graduate Research Center, Univ. of Mass., Box 34517, Amherst, MA, U.S.A.
[14] Northeast Radio Observatory Corp., Haystack Observatory, Westford MA 01886, U.S.A.
[15] NRAO, Socorro NM 87801, U.S.A.

Received July 3, 1997; accepted March 19, 1998

Abstract. We present 15 images from the global mm-VLBI sessions in 1990 April at 100 GHz and 1993 April at 86 GHz. These observations probe the central engines of the 16 observed AGN's with up to 50 μas resolution. Among other sources previously observed with $\lambda 3$ mm VLBI we present the first $\lambda 3$ mm maps of 0735+178, 0748+126, 1055+018, 2145+067, and CTA 102, in total we have been able to image 13 out of the 16 observed sources. 6 out of the 13 imaged sources observed exhibit curvature and rapid structural changes, although the low dynamic range in two thirds of the maps limits the detection of weak features. Most of the sources have unresolved cores even at this high resolution. There is substantial evidence that the observed sources can be grouped into two general groups: A misaligned population with parsec scale jets in the form of low pitch helices and an aligned population with straight jets with small changes in PA due to intrinsic bends.

Key words: galaxies: jets — radio continuum: galaxies — galaxies: active — galaxies: nuclei

Send offprint requests to: F.T. Rantakyrö
⋆ *Present address:* SEST/ESO, Casilla 19001, Santiago 19, Chile.

1. Introduction

The 1988 session was the first epoch where we could produce hybrid maps using intercontinental baselines to obtain a resolution of 50 μas. This could be achieved because of the development of new receivers, improved phase stability of local oscillators, and new data reduction techniques (Bååth et al. 1992). Since 1988 until and including the epochs presented here we have observed four epochs, in March 1988, March 1989, April 1990, and April 1993. These observations involved telescopes in Europe, Japan, Chile, and U.S.A. The 1988 and 1989 epochs have been previously published (Bååth et al. 1991 and Bååth et al. 1992). This paper presents the results from the 1990 and 1993 epochs. Our main aim with these observations is to obtain the highest possible resolution to be able to image the vicinity of the AGN core and the base of the jet emerging from the core.

Our observations so far have shown that the radio cores of the most powerful of the AGN's are very small, on the order of $10^{16} - 10^{17}$cm, which is only $5 - 500$ times larger than the Schwarzschild radius of a 10^9 $M_\odot$ black hole and of the same size scale as the non-thermal source observed by Band & Malkan (1989). A special and characteristic feature of the sub-milliarcsecond scale structures is that

the curvature observed with cm-VLBI seems to continue, but is further enhanced, closer to the core.

Typical for the major outbursts we observe from AGN's is that they first start with a rapid increase in intensity simultaneously (Courvoisier et al. 1988) at optical-IR and later at high radio frequencies (86 GHz and higher). High frequency single dish monitoring shows that outbursts tend to emerge almost simultaneously over the range $86 - 300$ GHz with turnover frequency reaching 86 GHz within a month and then 22 GHz within $4 - 5$ months (Lainela et al. 1993; Stevens et al. 1996). Similar time scales are observed in 3C 279 (Litchfield et al. 1995). This has been explained (Marscher & Gear 1985; Marscher et al. 1993) by a thin shock which is formed close to the central engine and then moves down the jet. After some time the shock will expand adiabatically and the spectral turnover (due to synchrotron self-absorption) will move towards lower frequencies. The outburst will therefore be observed at lower frequencies after the expansion has started. Observations of the shocks at their early stages of development are fundamental to our understanding of how they are formed, how they emerge from the core, and how they develop on their way through the radio jet. It must be emphasized that such observations can only be done with very high angular resolution at high frequencies.

It is clear that at present our λ3 mm observations suffers from lack of *uv*-coverage and has sensitivity problems, but we see this as the first step towards obtaining high dynamic range maps.

2. Observations and data reduction

The April 1990 session was a global 100 GHz mm-VLBI session involving the following telescopes: Hat Creek (U.S.A.), Kitt Peak (U.S.A.), Nobeyama (Japan), Onsala (Sweden), Owens Valley (U.S.A.), and SEST (Chile). The data was recorded on MarkIII-tapes using 14 IF-channels each with a 4 MHz bandwidth, and later correlated at the Haystack correlator. The raw output from the correlator were read into the AIPS package using specially written software (Bååth et al. 1992). The fringe finding and the necessary special post-processing to handle the interferometric mm-VLBI data are described by Bååth et al. (1992), in which a full description is given of the initial data processing stages done at the correlator. The 1990 and 1993 data were processed in exactly the same way. The amplitude calibration was done by applying the measured source flux density at each station, correcting for gain and atmospheric effects. We believe that the amplitudes are correct to within 30%. The discrepancy between the measured flux density in the maps and the estimated flux density at the shortest baselines (Table 2) is attributed to the generally poor *uv*-coverage. The lack of short *uv*-spacings not only causes additional noise in the maps, but can lead to spurious features in the maps which may be misidentified as components.

Table 1. Telescope information. D is the diameter in meters, μ is the sensitivity in Jy/K, $T_{\rm sys}$ the single-sideband system equivalent noise in Kelvin referred to outside the atmosphere, and the final column gives the sessions in which the telescope participated

Name	D [m]	μ [Jy/K]	$T_{\rm sys}$ K	Sessions
Effelsberg	100	7.7	800	93
Hat Creek	3×6.1	90	420	90
Haystack	37	17	400	93
Kitt Peak	12	53	205	90/93
Nobeyama	45	6	690	90/93
Onsala	20	35	480	90/93
Owens Valley	10.4	46	500	90/93
Quabbin	14	42	320	93
Sest	15	20	690	90/93
Pico Veleta	30	7.1	200	93

The later hybrid mapping and *uv* data model fitting were done in parallel in the AIPS and DIFMAP packages in order to have two different approaches to making the maps from the UV data and thus minimize the effects of sparse *uv*-sampling and mapping algorithms. We have been very careful to constrain the placement of source components by careful use of windowing techniques, to minimize the appearance of spurious features discussed previously. If the two methods yielded markedly different hybrid maps then both maps were discarded and we present only a model fit to the UV data.

The 1993 April observations were a global mm-VLBI experiment similar to the previous epoch but with the receivers tuned to 86 GHz. Telescopes participating in addition to those at the 1990 April session were: Effelsberg (Germany), Pico Veleta (Spain), and Quabbin (U.S.A.). The fringe finding, post-processing, and hybrid mapping followed the same procedures as for the 1990 April session. Information on the participating antennas can be found in Table 1.

The following sources yielded no fringes in either the 1990 April or the 1993 April experiments: 0016+731, 0133+476, 0212+735, 0235+164, 0234+285, 0300+471, 0458-020, 0528+134, 0642+449, 0716+714, 0748+126, 1012+232, 1044+719, 1116+128, 1156+295, 1308+326, 1334-127, 1354+196, 1413+135, 1418+546, 1611+343, 1633+382, 1637+574, 1642+690, 1716+686, 1749+096, 1802+784, 1803+784, 1823+568, 1928+738, 1954+513, 2005+403, 2007+777, 2021+317, 2201+315, 2234+282, 3C 286, 3C 274, 3C 371, 3C 380, 4 C 39.25, 4C 67.05, 4C 71.07, Centaurus A, Cygnus A, Cygnus X-3, DA 193, NRAO 140, NRAO 150, NRAO 512, NRAO O530, OA 129, and Saggitarius A. Since the observations were limited to only one or a few scans it is not surprising that later observations with more scans have found fringes to some of these sources (Krichbaum et al. 1996a; Alberdi et al. 1997;

Table 2. Basic source information for the April 90 and April 93 sessions for sources that yielded fringes. Positions are in the J2000.0 coordinate system, z is the cosmological redshift, m_v is the mean visual magnitude, $\mathrm{Flux_{VLBI}}$ is the source flux density inferred from the shortest (continental) baselines, and $\mathrm{Flux_{SD}}$ is the measured single dish flux density at $\lambda 3$ mm at the time of the observations. Where available the information has been given for both the 90 and 93 epochs. Positions, redshift, morphological type, and m_v are taken from the NED database

Source	α	δ	redshift [z]	Morph Type	m_v	$\mathrm{Flux_{VLBI}}$ [$\mathrm{Jy_{90}/Jy_{93}}$]	$\mathrm{Flux_{SD}}$ [$\mathrm{Jy_{90}/Jy_{93}}$]
3C 84	031948.160	+413042.103	0.0172	cD/SyII	12.64	1.8/3.0	13.3/-
3C 111	041821.326	+380135.676	0.0485	N Galaxy/SyI	18.0	-/1.2	-/-
0420−014	042315.801	−012033.063	0.915	OV/HPQ	17.76	1.8/-	4.2/2.6
0735+178	073807.394	+174218.993	0.424	BL Lac/OV	14.85	2.5/-	2.6/1.35
0748+126	075052.046	+123104.832	0.281/0.889	-	17.8	-/1.4	
OJ 287	085448.875	+200630.639	0.306	BL Lac/OV	14	2.0/1.2	3.9/1.6
1055+018	105829.605	+013358.828	0.888	BL Lac/OV; HPQ	18.28	2.2/-	4.3/3.0
3C 273B	122906.700	+020308.596	0.158	OV/LPQ	12.86	3.5/-	29.4/26.3
3C 279	125611.167	−054721.539	0.538	OV/HPQ	17.75	3.0/3.5	12.7/20.0
1510−089	151250.533	−090559.824	0.360	OV/HPQ/Sy I	16.52	4.0/-	3.5/3.35
3C 345	164258.810	+394837.000	0.593	OV/HPQ	15.96	2.0/-	3.2/-
2145+067	214805.459	+065738.606	0.990	OV/LPQ	16.47	-/1.4	4.2/5.3
BL Lac	220243.291	+421639.984	0.0686	BL Lac/OV	14.5	2.2/-	2.2/-
3C 446	222547.259	−045701.394	1.404	BL Lac/OV/HPQ	17.19	5.0/-	9.3/2.3
CTA 102	223236.409	+114350.902	1.037	OV/HPQ	17.33	3.8/-	-/1.55
3C 454.3	225357.748	+160853.565	0.859	OV/HPQ	16.1	7.0/-	7.4/8.0

Krichbaum et al. 1994; Standke et al. 1994; Schalinski et al. 1994).

3. Results

Table 2 contains the basic source information for the 1990 April and 1993 April sessions for sources that yielded fringes at either or both epochs. The table gives the positions in the J2000.0 coordinate system, the cosmological red-shift, the optical magnitude, the source flux density inferred from the shortest baselines ($\mathrm{Flux_{VLBI}}$), and the measured single dish flux density ($\mathrm{Flux_{SD}}$) at $\lambda 3$ mm (Tornikoski et al. 1996) where this information is available for the source in question. Table 3 contains more detailed source information. It gives the maximum observed proper motion in the source (Vermeulen & Cohen, 1994 and references therein), measured X-ray (Della Ceca et al. 1990), and maximum observed γ-ray fluxes for photon energies >100 MeV (Chiang et al. 1995; Lin et al. 1993; Montigny et al. 1995). For all mapped sources we present the maps with a 50μas circular beam if the original beam is within 10% of this value. The size of the convolving beam was chosen to be able to compare with the previously published maps (Bååth et al. 1992). Table 4 gives the UV data information. It gives the number of scans with closure phase data and the length of time over which the sources was observed for the epochs in question.

Table 3. Source information. μ, is the maximum proper motion observed in this source at lower frequencies. F_{X} is the measured X-ray flux, and F_γ is the maximum observed γ-ray flux for photon energies >100 MeV

Source	μ [mas/yr]	F_{X} [μJy]	F_γ [10^{-8} photons cm^{-2} s^{-1}]
3C 84	0.54 ± 0.12	18	<9
3C 111	1.54 ± 0.2	-	<9
0420−014	-	0.52	45
0735+178	0.44 ± 0.03	0.3	28 ± 9
0748+126	-	-	-
OJ 287	0.27 ± 0.03	3	-
1055+018	-	-	-
3C 273B	1.15 ± 0.15	12	30
3C 279	0.5 ± 0.1	3.4	270
1510−089	-	0.84	27 ± 6
3C 345	0.47 ± 0.02	0.6	13 ± 6
2145+067	-	-	-
BL Lac	1.2 ± 0.1	<1	-
3C 446	0 ± 0.06	1.0	-
CTA 102	0 ± 0.5	0.75	46
3C 454.3	0.35 ± 0.06	1.46	135

3.1. 3C 84

The radio source is identified with the dominant disturbed elliptical galaxy in the Perseus cluster. It has been detected as a strong diffuse X-ray source with a strong X-ray point source coincident with the radio core. The radio frequency morphology is quite complicated (Krichbaum et al. 1992; Venturi et al. 1993) exhibiting

Table 4. UV data information. Scans, are the number of scans with closure phase information and Time, is the length of time over which the scans where found. The 1990 epoch used an observing scheme where the data were recorded for 6.5 minutes and followed by a 23.5 minutes idle time giving 30 minutes for one observation cycle. With more tapes available for the 1993 epoch, the idle time was only 6.5 minutes giving a total observation cycle of 15 minutes

Source	Epoch [yr]	Scans	Time [hours]
3C 84	90	6	23
	93	16	11
3C 111	93	8	2
0420−014	90	1	0.5
0735+178	90	7	4
0748+126	93	2	0.5
OJ 287	90	5	2.5
	93	6	1.5
1055+018	90	4	3
3C 273B	90	7	6
3C 279	90	18	9
	93	42	10.5
1510−089	90	2	1
3C 345	90	6	6
2145+067	93	20	5
BL Lac	90	22	12
3C 446	90	9	7
CTA 102	90	1	0.5
3C 454.3	90	1	0.5

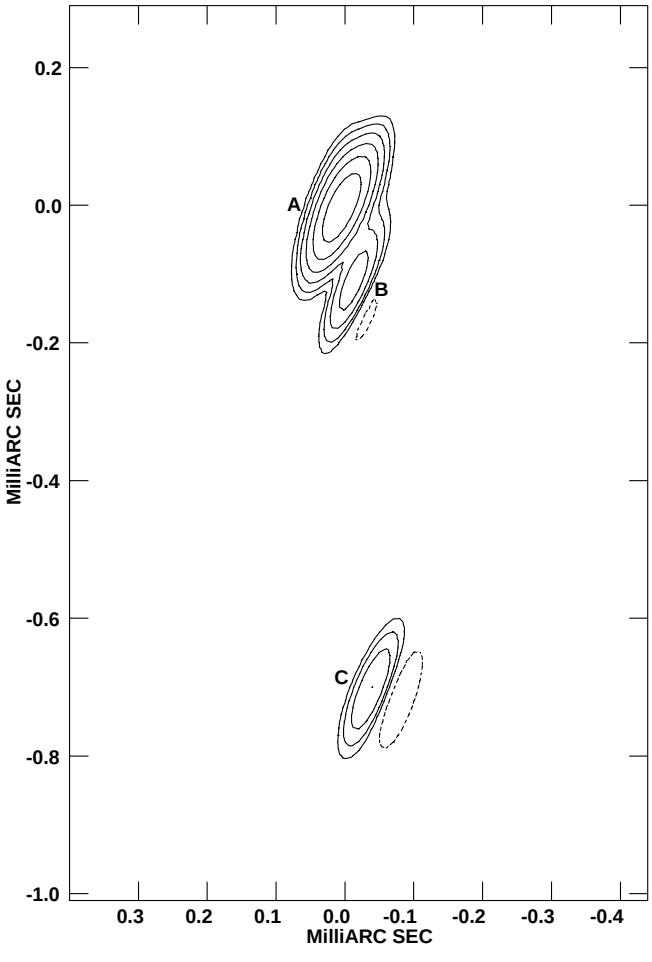

Fig. 1. 3C 84 100 GHz map from 1990 April 21. Peak flux density = 1.1 Jy/Beam. Contour intervals are chosen as (−2.0, 2.0, 4.0, 8.0, 16.0, 32.0, 64.0,128.0) × 10 mJy/beam. In this and succeeding figures, negative contours, if any, are shown dashed. The restoring beam was a elliptical Gaussian (0.12 × 0.03 mas in PA = −21.3°)

a core with two opposite radio-jets, with the southern jet consisting of components moving down a diffuse jet and finally expanding into an amorphous component at 12 mas. Krichbaum et al. (1992) showed that the inner jet components move with 0.1c and that after a major bend the jet speed accelerated. λ7 mm VLBI observations (Krichbaum et al. 1993) show a complex structure with 6 components embedded in an extended jet. The 3 mm (US-only), epoch march 1987 map by Wright et al. (1988) exhibits a core with a jet in PA $\sim$ 230°. Embedded in the jet at $r \sim 0.3$ mas is a second component. The previous λ3 mm observations (Bååth et al. 1992) showed a core with a component moving out with $\mu = 85 \pm 7\,\mu$as/year with diffuse components 0.5 mas south of the core. In the 1989 map there is a hint of a ridge-line connecting the components but the dynamic range is not sufficient to clearly show the underlying flow. The 1990 epoch map (Fig. 1) has a structure very similar to that seen at the previous epochs. A core extended in PA $\sim -90°$(A) with two components well separated from the core, one in PA $\sim 200°$ at $r \sim$150 μas(B) and the other in PA $\sim 180°$ at $r \sim 0.7$ mas(C). This structure agrees very well with that seen at the previously published epochs (Wright et al. 1988; Bååth et al. 1992). The 1993 map (Fig. 2) has a unresolved core(A) and two components in PA $\sim 180°$, one extended component at $r \sim 0.35$ mas(D) and a weak component at $r \sim 0.8$ mas(E). With 3 years between the epochs it is not surprising that the structure has changed dramatically. Looking at the three epochs from 1989 to 1990 it appears as if the components leave the core in a PA $\sim -100°$, and later turn to the south. In Table 2 it is clear that most of the total flux density is resolved out, and that our λ3 mm maps probe only the most compact structures, leaving the flux density and position of more extended emission ill constrained. This fact is valid for most of the sources presented in this paper unless specified otherwise. The structures in both maps were too complicated to allow a Gaussian model fit to the *uv* data, as the fitting program has severe problems fitting more than three components to a *uv* data set. Thus we present

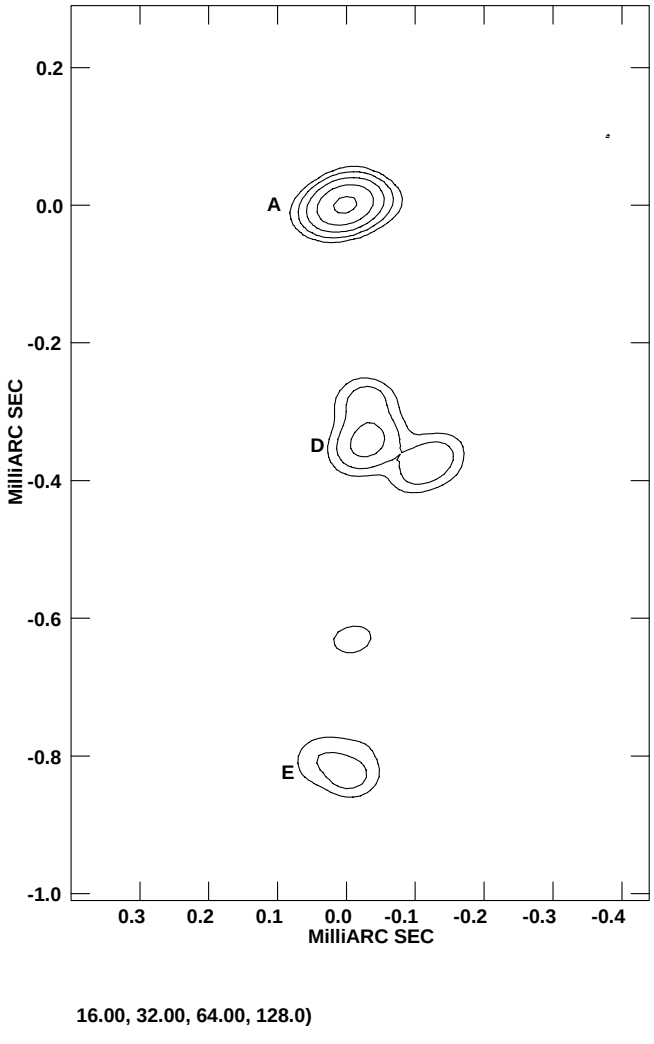

Fig. 2. 3C 84 86 GHz map from April 4, 1993. Peak flux density = 0.74 Jy/Beam. Contour intervals are chosen as (−4.0, 4.0, 8.0, 16.0, 32.0, 64.0, 128.0) × 10 mJy/beam. The restoring beam was a elliptical Gaussian (0.07 × 0.05 mas in PA = −68.7°)

Table 5. Model parameters for Gaussian components fitted to the 3C 84 maps for sessions 90 and 93. Flux is the flux density of the component, $\Delta\alpha$ and $\Delta\delta$ gives the position of the component relative to the core, Size is the size of the fitted Gaussian, PA is the Position Angle of the major axis of the fitted Gaussian. The errors represent $3\,\sigma$ from the fit

	Yr	Flux [Jy]	$\Delta\alpha$ [μas]	$\Delta\delta$ [μas]	Size [μas]	PA [°]
A	90	1.12 ± 0.02	-	-	<40	-
B	90	0.25 ± 0.02	−20 ± 5	−124 ± 5	<30	-
C	90	0.17 ± 0.02	−40 ± 5	−700 ± 5	<50	-
A	93	0.74 ± 0.02	-	-	<30	-
D	93	0.16 ± 0.03	−54 ± 5	−343 ± 15	150 × 50	55 ± 5
E	93	0.12 ± 0.02	6 ± 5	−820 ± 5	<80	

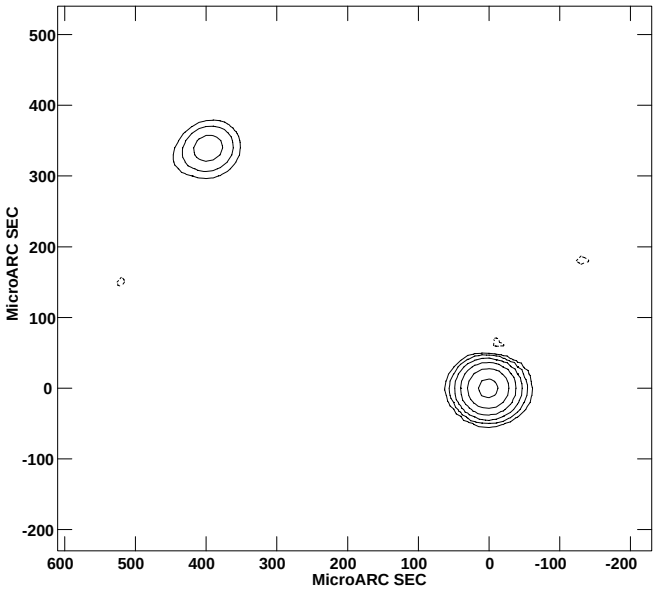

Fig. 3. 3C 111 86 GHz map from April 4, 1993. Peak flux density = 0.8 Jy/Beam. Contour intervals are chosen as (−4.0, 4.0, 8.0, 16.0, 32.0, 64.0) × 10 mJy/beam. The restoring beam was a 0.05 mas (FWHM) circular Gaussian

the result of fitting Gaussian components to the images (Table 5). As the positions of the components are the result from fitting to the image we have also labelled the components in the two maps. It is clear from Figs. 1 and 2 that there are drastic internal structural changes in the source. The long time between epochs makes identification difficult, but we will make some simple assumptions to try to quantify these structural changes. If we assume that component D is component B seen at a later epoch and making the same assumption for components C and E, we get a proper motion of $70 \pm 20\mu$as/year for component B and 40 ± 10 μas/year for component C. These values agree well with the velocities seen by Bååth et al. (1992). If component B is the result of a component leaving the core after the March 1989, as suggested by the extension in PA $\sim -135°$ in the March 1989 map (Bååth et al. 1992) and the observed increase in flux density, then we can estimate the proper motion to be $\sim 130 \pm 20$ μas/year.

3.2. 3C 111

This is a classical double-lobed FRII radio-source with an extended jet in PA $\sim -45°$ (Preuss et al. 1990). Components are seen moving out from the core at superluminal velocities ∼1 mas/year. In Fig. 3 we present the highest resolution map of this source available to this date. The core is unresolved and there is a weak component in

Table 6. Model parameters for the Gaussian components fitted to the 3C 111 *uv* data. Explanation of parameters can be found in Table 5

	Year	Flux [Jy]	$\Delta\alpha$ [μas]	$\Delta\delta$ [μas]	Size [μas]
A	93	0.9 ± 0.1	-	-	<50
B	93	0.2 ± 0.1	400 ± 20	340 ± 20	<50

Table 7. Model parameters for Gaussian components fitted to the 0420−014 UV data. Explanation of parameters can be found in Table 5

	Year	Flux [Jy]	$\Delta\alpha$ [μas]	$\Delta\delta$ [μas]	Size [μas]
A	90	1.8 ± 0.3	-	-	<100

the same PA as the mas scale jet at a distance of 0.5 mas. The result from model fitting Gaussian components to the UV data can be found in Table 6.

The Gaussian model fit clearly substantiates the general structure presented in the hybrid map. With only one epoch we are unable to determine whether the superluminal motion seen at lower frequencies (Preuss et al. 1990) is present on μas scales. Further observations are needed to detect the possible proper motion of components in this source.

3.3. 0420−014

This source is a radio-loud flat-spectrum AGN and also classified as a Blazar. It has been detected in γ and X-rays (Radecke et al. 1995), and has a very high optical polarization of ∼17% (Wills et al. 1992). At mas resolution the source shows a symmetrical unresolved core. This is the case of either a "naked" core or that of a jet aligned very close to the line of sight (Wehrle et al. 1992). At λ7 mm the source consists of a core and a pronounced bent jet (Krichbaum et al. 1994a). We found fringes to the source in 1990 for one scan which was not enough to make a hybrid map but sufficient to make a fit to the UV data. The result of the model fit is presented in Table 7.

Comparing with the $\mathrm{Flux_{SD}}$ (Table 2), it is clear that more than 50% of the flux density is missing. With so few *uv* points covering such a short time it is difficult to make any statements about the source structure, but it is clear that this source *is* observable at λ 3 mm, and warrants further observations.

3.4. 0735+178

This source is a BL Lac object which is point-like in the optical and with arcsec resolution at radio wavelengths. VLBI polarization observations at 6 cm show that the core has a high degree of polarization, $\gtrsim$3% (Gabuzda et al. 1994). At mas resolution the source has an unresolved core and a jet extending to the NE (Bååth & Zhang 1991), with components moving at superluminal velocities. The components appear to follow different paths as they move out from the core (Gabuzda et al. 1994). Our April 90 map, the first ever of this source with μas resolution, shows (Fig. 4) two components but it is not clear which is the core. There are no significant features outside the region shown. The result from model fitting Gaussian components to the UV data can be found in Table 8.

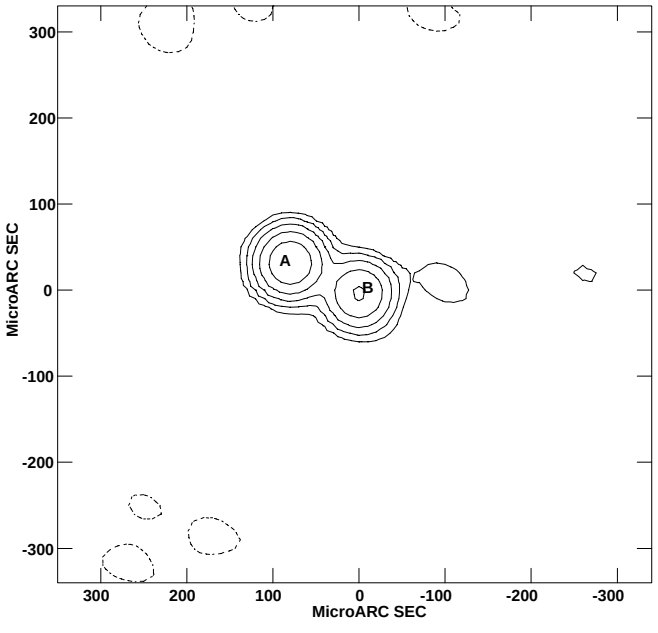

Fig. 4. 0735+178 100 GHz map from April 20, 1990. Peak flux density = 1.2 Jy/Beam. Contour intervals are chosen as (−2.0, 2.0, 4.0, 8.0, 16.0, 32.0, 64.0) × 20 mJy/beam. The restoring beam was a 0.05 mas (FWHM) circular Gaussian

Table 8. Model parameters for Gaussian components fitted to the 0735+178 UV data. Explanation of the parameters can be found in Table 5

	Year	Flux [Jy]	$\Delta\alpha$ [μas]	$\Delta\delta$ [μas]	Size [μas]
A	90	1.1 ± 0.2	-	-	<50
B	90	1.0 ± 0.2	−140 ± 10	−80 ± 10	<50

As with 3C 111 we have a good agreement between the hybrid map and the model fitting. Almost all of the $\mathrm{Flux_{SD}}$ (Table 2) is seen in our map suggesting that most if not all high frequency flux density is emitted from this central region. Having only one epoch available we can say nothing about the superluminal motion in this source at μas scales. Assuming that component B is the "core" the jet is straight from μas to mas scales; if component A

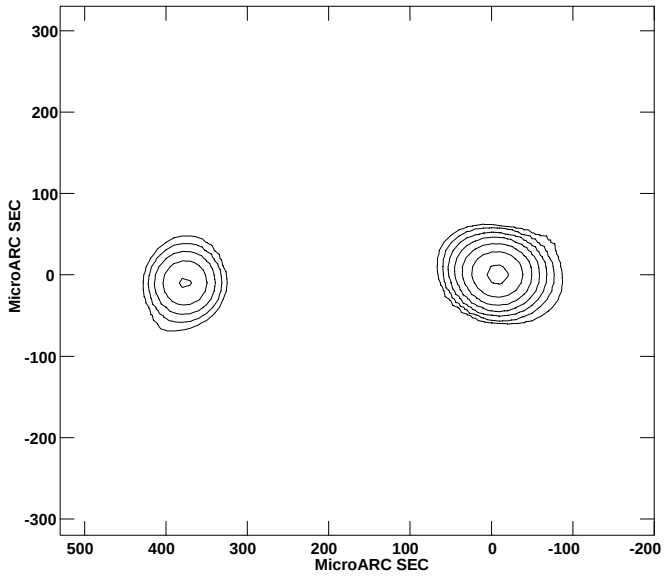

Fig. 5. 0748+126 86 GHz map from April 4, 1993. Peak flux density = 0.8 Jy/Beam. Contour intervals are chosen as (−2.0, 2.0, 4.0, 8.0, 16.0, 32.0, 64.0) × 10 mJy/beam. The restoring beam was a 0.05 mas (FWHM) circular Gaussian

is the "core", this would indicate a sharp twisting of the jet from μas to mas scales. The identity of the "core" is currently unknown.

3.5. 0748+126

This is an unclassified QSO whose redshift is ambigous; two possible redshifts are suggested by Wills & Wills (1976): $z = 0.281$ or $z = 0.88$. VLA observations (Murphy et al. 1993) show an unresolved core with several components in PA $\sim 135°$ connected by a slightly bent jet.

The first map of this source made with λ3 mm VLBI is presented in Fig. 5. The map also shows an unresolved core with a component in PA $\sim 90°$ at 0.37 mas. The weak components do not lie in the general PA of the VLA map, but as in many other sources this is not an uncommon feature (see 3C 345, 3C 446, OJ287, BL Lac, and CTA 102 in this paper). With no single dish monitoring available for this source at this epoch we cannot make any conclusions concerning the degree of missing flux density. To test the fidelity of the hybrid map we also made a Gaussian model fit to the UV data. The best fit is presented in Table 9, which confirms the flux densities and location of components seen in the hybrid map.

Table 9. Model parameters for Gaussian components fitted to the 0748 + 126 UV data. Explanation of the parameters can be found in Table 5

	Year	Flux [Jy]	$\Delta\alpha$ [μas]	$\Delta\delta$ [μas]	Size [μas]
A	93	1.0 ± 0.3	-	-	<50
B	93	0.3 ± 0.2	350 ± 90	80 ± 20	<50

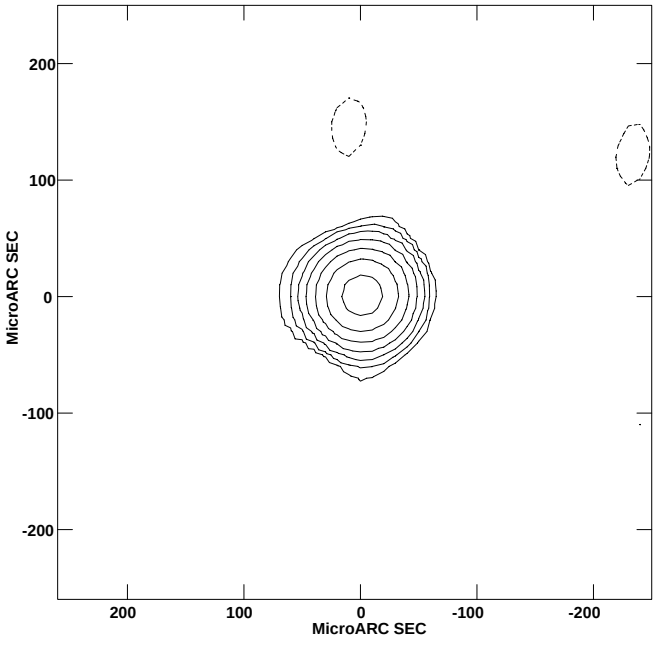

Fig. 6. OJ 287 100 GHz map from April 21, 1990. Peak flux density = 1.7 Jy/Beam. Contour intervals are chosen as (−2.0, 2.0, 4.0, 4.0, 8.0, 16.0, 32.0, 64.0, 128.0) × 10 mJy/beam. The restoring beam was a 0.05 mas (FWHM) circular Gaussian

3.6. OJ287

This is a prominent member of the BL Lac class with highly varying flux densities in both the optical and radio regimes. The variability time-scales vary from minutes to years (Takalo 1994; Aller et al. 1985). The source exhibits superluminal expansion along PA $\sim -110°$ (Roberts et al. 1987; Gabuzda et al. 1989). Model-fitting to the 7 mm VLBI data (Krichbaum et al. 1993) yields a two component model with the second component at 0.9 mas in PA = 232°. The previous two epochs (Bååth et al. 1992) show an unresolved core. The April 1990 map (Fig. 6) shows an unresolved core. The *uv* data for this epoch has been discussed extensively by Tateyama et al. (1996). Here we include the map for completeness. In 1993 (Fig. 7) the core is still unresolved and there is a component in PA $\sim -45°$ at 0.05 mas. Most of the single dish flux density (Table 2) is seen in our map, the missing flux density

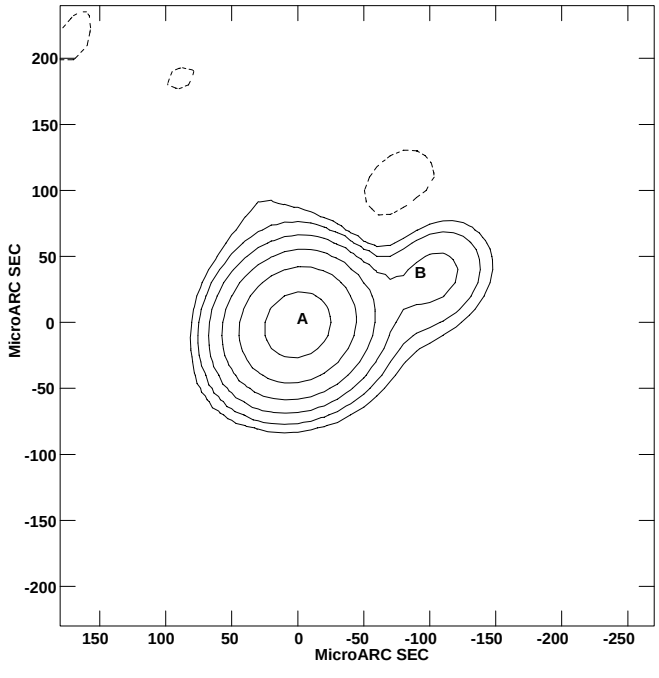

Fig. 7. OJ 287 86 GHz map from 1993 April 4. Peak flux density = 0.9 Jy/Beam. Contour intervals are chosen as (−1.0, 1.0, 2.0, 4.0, 8.0, 16.0, 32.0, 64.0) × 10 mJy/beam. The restoring beam was a 0.05 mas (FWHM) circular Gaussian

Table 10. Model parameters for Gaussian components fitted to the OJ 287 UV data. Explanation of the parameters can be found in Table 5

	Year	Flux [Jy]	$\Delta\alpha$ [μas]	$\Delta\delta$ [μas]	Size [μas]
A	90	1.8 ± 0.3	-	-	25 × 25
A	93	0.9 ± 0.2	-	-	< 50
B	93	0.13 ± 0.10	−99 ± 25	26 ± 24	<50

may be the result of either incorrect calibration and/or resolution effects. In the three years between the observations the $\mathrm{Flux_{VLBI}}$ has decreased by 40%. We attribute the decrease in observed flux density to component B moving out from the core and decreasing in strength. The result from the Gaussian model fit to the uv data can be found in Table 10.

There is a good agreement between the hybrid maps and the Gaussian model fits at both epochs. Assuming that component B has moved out from the core after the 1990 April epoch, we can obtain a lower limit to its proper motion. In the 1993 April map, component B lies at $r \sim 102 \pm 35$ μas, thus it has moved with a minimum proper motion of 34 μas/year. Our λ3 mm data suggests that components leave the core in PA $\sim -45°$ and later turn to PA $\sim -110°$ on mas scales.

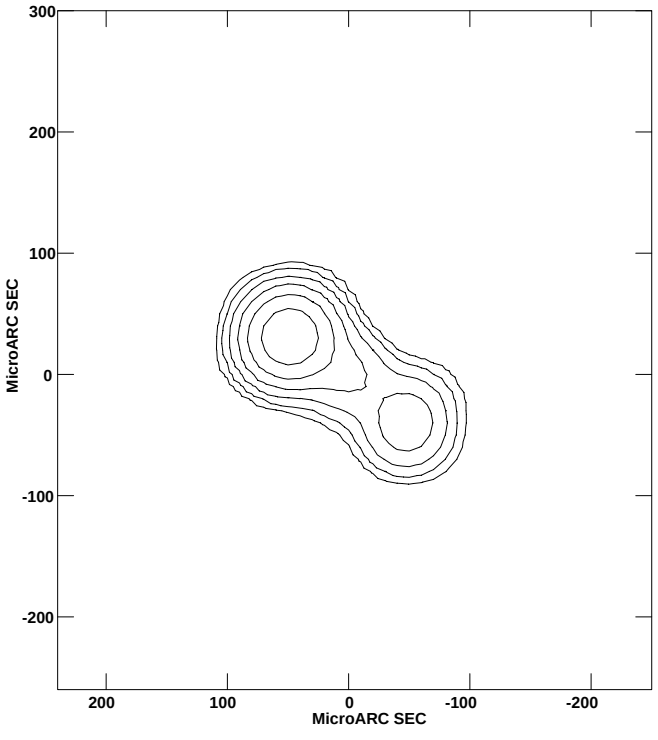

Fig. 8. 1055+018 100 GHz map from April 20, 1990. Peak flux density = 1.11 Jy/Beam. Contour intervals are chosen as (−1.0, 1.0, 2.0, 4.0, 8.0, 16.0, 32.0, 64.0) × 10 mJy/beam. The restoring beam was a 0.05 mas (FWHM) circular Gaussian

3.7. 1055+018

This source has a core-jet structure at mas resolution (Bondi et al. 1996) with a 15 mas jet extended in PA ~ -65 and a weak component at ∼25 mas in the same general PA. On arcsec scales the source has a triple structure, a strong central component and two diffuse lobes in a NS direction. The southern feature is connected to the central bright component with a bent jet (Murphy et al. 1993). Figure 8 shows the first 50 μas map of this source. The hybrid map shows an unresolved core with an extended jet in PA $\sim -135°$. As for OJ 287, half of the single dish flux density (Table 2) is lost in the mmVLBI map, suggesting that the missing flux density is emitted from the jet which is resolved out in our map. To test the hybrid map we tried model fitting Gaussian components to the uv data. The best fit is presented in Table 11.

The hybrid map and the Gaussian model fit disagree in the exact location and the flux densities of the two components. Both models have two strong components separated by $\sim 150 - 200$ μas. The Gaussian model fit places the second component more to S than in the map. We conclude that the sparse UV coverage makes the interpretation of the data very difficult. Observations with fuller

Table 11. Model parameters for Gaussian components fitted to the 1055+018 UV data. Explanation of the parameters can be found in Table 5

	Year	Flux [Jy]	$\Delta\alpha$ [μas]	$\Delta\delta$ [μas]	Size [μas]
A	90	2.2 ± 0.6	-	-	<50
B	90	1.4 ± 0.6	−46 ± 30	−240 ± 60	<50

uv-coverage are needed to determine its exact structure. For now we conclude that the data supports a structure with two strong components separated by ∼175 μas.

3.8. 3C 273B

This quasar is a classical superluminal source (Zensus 1987). The mas jet can be seen extending from the core out to more than 150 mas (Unwin 1990), and the PA of this jet is well aligned with the arc-second scale jet (Davis et al. 1985). VLBI monitoring of this source at λ1.3 cm (Zensus et al. 1990) shows two features moving out from the core, with $\mu = 0.65$ and $\mu = 0.92$ mas/yr respectively. A prominent feature is the twisting of the jet, seen in both total intensity maps and polarization maps (Leppänen et al. 1995), with an increase in polarization with distance from the core.

A 3 mm observation made by Krichbaum et al. (1990), showed jet components being ejected after a major optical outburst. Bååth et al. (1991) showed a core with a bent jet, with several components at different PA's, suggesting that the wiggling seen at mas scales continued at μas scales. The 1988 map showed an elongated component emerging at the time, which could be related to an outburst, seen 60 days earlier in Optical/IR (Courvoisier et al. 1988). Krichbaum et al. (1996b) showed 2 new epochs (1994 & 1995) which clearly show the fast (0.5 − 0.6 mas/yr) superluminal motion in 3C 273.

The 1990 map (Fig. 9) shows an unresolved core and a component in the same PA as seen in earlier 3 mm maps of this source. We do not see the other components but they may be too weak to be detected with the limited dynamic range we have in this map. Most of the single dish flux density (Table 2) is missing, suggesting that the major part of the λ3 mm flux density is emitted by the extended jet. The result from a Gaussian model fit to the UV data can be found in Table 12. Both methods agree on the general location and flux densities of the fitted components.

We are unable to determine the proper motion in this source as the previous epoch map was made in 1998 March and the structural changes have been too large to identify the components and determine their motions.

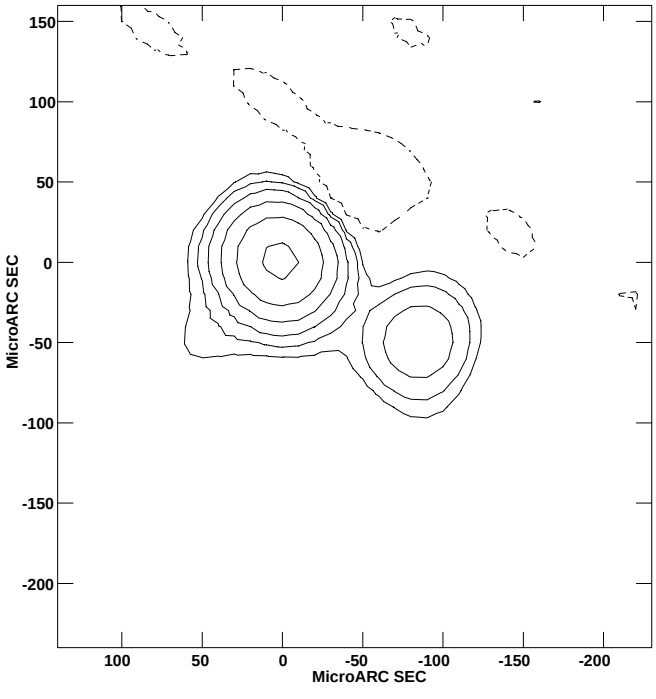

Fig. 9. 3C 273B 100 GHz map from April 20, 1990. Peak flux density = 3.0 Jy/Beam. Contour intervals are chosen as (−8.0, 8.0, 16.0, 32.0, 64.0, 128.0, 256.0) × 10 mJy/beam. The restoring beam was a 0.05 mas (FWHM) circular Gaussian

Table 12. Model parameters for Gaussian components fitted to the 3C 273B UV data. Explanation of the parameters can be found in Table 5

	Year	Flux [Jy]	$\Delta\alpha$ [μas]	$\Delta\delta$ [μas]	Size [μas]
A	90	2.7 ± 0.3	-	-	<50
B	90	0.4 ± 0.3	−90 ± 30	−130 ± 30	<50

3.9. 3C 279

This has been one of the most frequently observed sources since it was the first radio object to exhibit superluminal motion (Whitney et al. 1971). Cotton (1979) confirmed the superluminal motion with a series of observations showing a expansion velocity of 0.5 mas/yr in PA ∼ −140. Later observations showed lower expansion speeds ∼0.15 mas/yr (Unwin et al. 1989; Carrara et al. 1993). The arcsec structure is a jet extending out to 10 arcsec in PA ∼ −145° (de Pater & Perley 1983); the jet is straight from mas to arcsec scale.

From being a moderately strong source in radio to γ-rays the source increased in flux density drastically such that in 1992 it was the brightest extra-galactic γ-ray source in the sky (Maraschi et al. 1994).

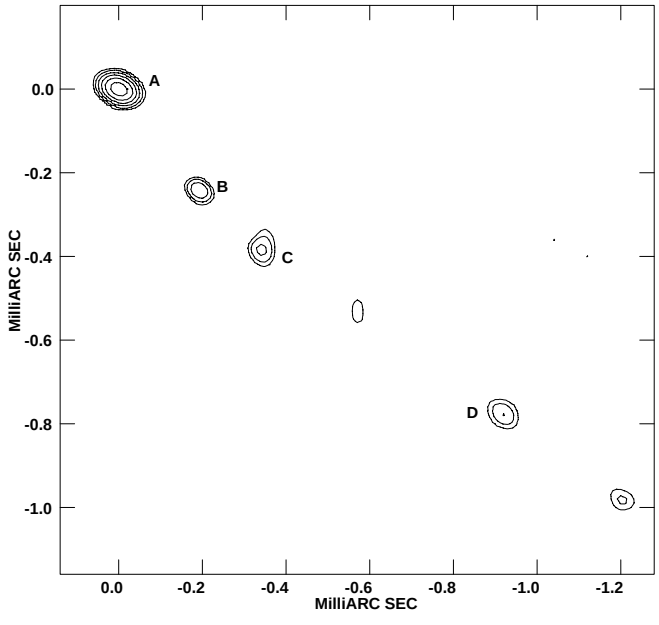

Fig. 10. 3C 279 100 GHz map from April 21, 1990. Peak flux density = 2.0 Jy/Beam. Contour intervals are chosen as (−4.0, 4.0, 8.0, 16.0, 32.0, 64.0, 128.0) × 10 mJy/beam. The restoring beam was a 0.05 mas (FWHM) circular Gaussian

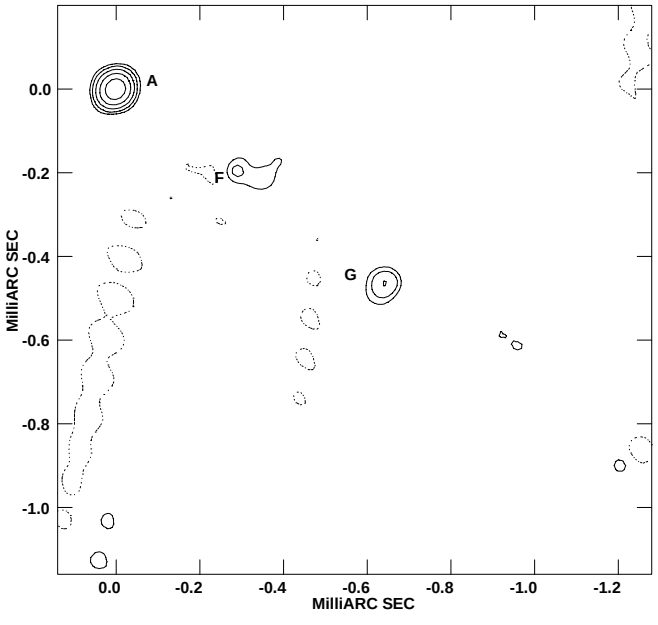

Fig. 11. 3C 279 86 GHz map from April 4, 1993. Peak flux density = 1.1 Jy/Beam. Contour intervals are chosen as (−4.0, 4.0, 8.0, 16.0, 32.0, 64.0, 128.0) × 10 mJy/beam. The restoring beam was a 0.05 mas (FWHM) circular Gaussian

The previous epoch observations (Bååth et al. 1992) showed a strong core with two weak components. That paper gave an estimated proper motion (0.15 mas/yr) which agrees with that seen at much lower frequencies. Our 100 GHz map from April 1990 (Fig. 10) has a similar structure to that seen in 1989. With the improved UV-coverage we are able to map the source from μas to mas scales. The PA of the components agree very well with the PA seen at mas scales (Carrara et al. 1993). The 1993 epoch map (Fig. 11) shows an unresolved core with two strong components in PA $\sim -145°$. The differences in position of the components at the two epochs clearly demonstrates structural changes in the source. Comparing the $\mathrm{Flux_{SD}}$ with $\mathrm{Flux_{VLBI}}$ (Table 2) shows that the λ3 mm emission of this source, like 3C 273, is strongly dominated by the extended jet. As for 3C 84 the structure is to complicated to make a Gaussians model fit to the UV data. The result of fitting Gaussian components to the images can be found in Table 13. As the positions of the components are the result of fitting to the image we have also labelled the components in the two maps.

The large separation in time between the April 1990 and April 1993 epochs and the apparent rapid structural changes makes identification and determination of proper motion using only these two maps very difficult. Fortunately we have the March 1989 map which is only separated by a year from our 1990 map. Assuming that component B in the April 1990 map is the outermost component seen in the March 1989 map, labelled $F2$ (Bååth et al. 1992), we estimate the proper motion to be $\mu \sim 80 \pm 10$ μas/year. This is a lower value than previously seen at μas scales, but our value should be seen as a lower limit to the proper motion, as it is based on the conservative assumption that component B has moved from the position of $F2$ and not from the core, labelled F in the 1989 map.

Table 13. Model parameters for Gaussian components fitted to the 1990 and 1993 maps of 3C 279. Explanation of the parameters can be found in Table 5

	Yr	Flux [Jy]	$\Delta\alpha$ [μas]	$\Delta\delta$ [μas]	Size [μas]	PA [°]
A	90	2.0 ± 0.1	-	-	20 × 10	76 ± 6
B	90	0.31 ± 0.02	−193 ± 5	−240 ± 5	<20	-
C	90	0.20 ± 0.02	−340 ± 5	−380 ± 5	<40	-
D	90	0.16 ± 0.02	−920 ± 5	−780 ± 5	40 × 20	32 ± 10
A	93	1.11 ± 0.02	-	-	30 × 20	140 ± 10
F	93	0.09 ± 0.02	−330 ± 5	−200 ± 5	80 × 30	82 ± 10
G	93	0.17 ± 0.03	−640 ± 5	−470 ± 5	40 × 20	150 ± 20

3.10. 1510−089

VLBI observations at λ18 cm (Bondi et al. 1996) of this low frequency variable show a core-jet structure, with the

Table 14. Model parameters for Gaussian components fitted to the 1510−089 UV data. Explanation of the parameters can be found in Table 5

	Year	Flux [Jy]	$\Delta\alpha$ [μas]	$\Delta\delta$ [μas]	Size [μas]	PA [°]
A	90	4.0 ± 1.2	-	-	10 × 100	12 ± 4

jet extending 5 mas in PA $\sim 180°$. We found fringes to the source in 1990 for two scans, not enough to make a hybrid map, but sufficient to make a fit to the *uv* data. The result of the fit is presented in Table 14.

The resulting model fit has a Gaussian component elongated in NS, this elongation may very well be the result of poor *uv*-coverage and should not be interpreted as actual source structure.

3.11. 3C 345

The quasar 3C 345 has been observed over a large range of wavelengths, from radio to hard X–rays. Most of the total power of 3 10^{40} W is emitted in the sub-millimeter–optical domain, with one–sixth of the power radiated at radio and X–ray wavelengths (Bregman et al. 1986; Ku et al. 1980). At wavelengths longer than λ3 mm, the radio continuum spectrum is flat, but steepens at wavelengths shorter than 3 mm from a power–law of $\nu^{-0.91}$ over the band λ3 mm − λ30 μm, to $\nu^{-1.40}$ over λ30 μm − λ3 μm. 3C 345 has provided one of the best cases for superluminal expansion and acceleration (Unwin et al. 1983; Moore et al. 1983). Observations made at several epochs and wavelengths show that the components seem to move outwards along a helically curved jet (Biretta et al. 1986; Steffen et al. 1993; Zensus et al. 1995). Different components appear to follow different paths as they move out from the core (Steffen et al. 1993; Zensus et al. 1995). 7 mm maps made at the time between our two epochs (Krichbaum et al. 1993) show a core with several components at different PA's. The PA changes from $-45°$ at 0.2 mas to $\sim -130°$ at 3 mas. The 3 mm maps (Bååth et al. 1992) show a central feature assumed to be the core and components leaving the core in PA $\sim -45°$, and the jet changing PA to $\sim -135°$ at 0.4 mas, showing that the jet twists dramatically as it leaves the core. The source was detected in the 1990 session and shows (Fig. 12) an elongated core in PA $\sim -135°$. Comparison between $\mathrm{Flux_{SD}}$ and $\mathrm{Flux_{VLBI}}$ (Table 2) shows that this source like 1055+018 is largely resolved and that probably most of the missing flux density will be found on larger scales. The best model fit was achieved by using two Gaussian components. The actual location of the weaker component varied for model fits with similar rms, the location of the second component as presented in Table 15 is an average of these model fits.

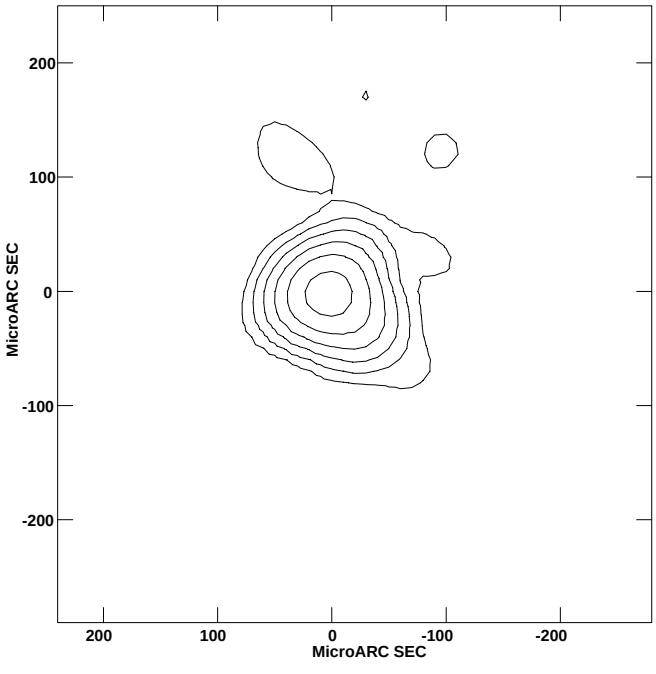

Fig. 12. 3C 345 100 GHz map from April 20, 1990. Peak flux density = 1.8 Jy/Beam. Contour intervals are chosen as (−4.0, 4.0, 8.0, 16.0, 32.0, 64.0, 128.0) × 10 mJy/beam. The restoring beam was a 0.05 mas (FWHM) circular Gaussian

Table 15. Model parameters for Gaussian components fitted to the 3C 345 UV data. Explanation of the parameters can be found in Table 5

	Year	Flux [Jy]	$\Delta\alpha$ [μas]	$\Delta\delta$ [μas]	Size [μas]
A	90	1.7 ± 1.2	-	-	<50
B	90	0.3 ± 0.2	−40 ± 40	−50 ± 40	<50

We conclude that both the image and the fits to the UV data confirms the existence of a second component in PA $\sim -90°$ although the exact position is not determined.

The poor quality of the April 1990 map makes determination of proper motions impossible. Component *B* could be component *E*3 from the April 1989 map, or a completely new component moving out from the core. With the available data we can only say that 3C 345 exhibits drastic structural changes even on timescales as short as a year.

3.12. 2145+067

Gregorini et al. (1984) showed that this object is a low frequency variable, which complicates the interpretation of the structure seen at lower frequencies. VLBI observations at 5 GHz (Wehrle et al. 1992) show a core extended

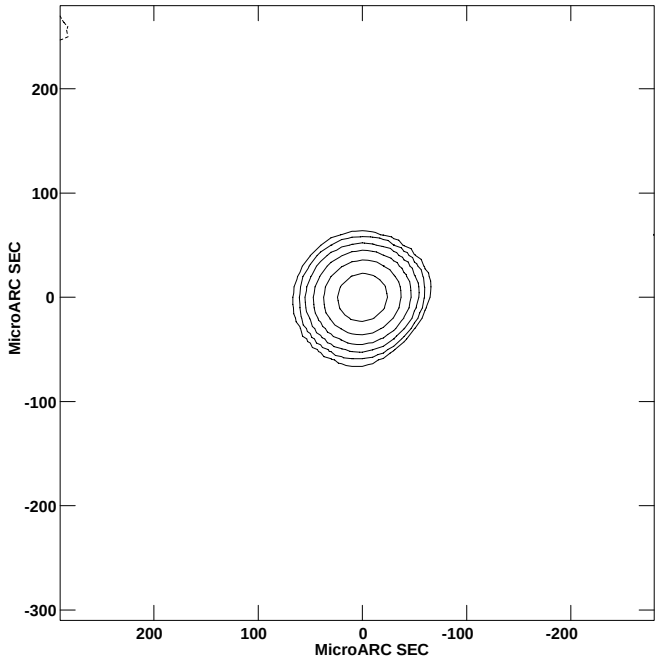

Fig. 13. 2145+067 86 GHz map from April 4, 1993. Peak flux density = 1.05 Jy/Beam. Contour intervals are chosen as (−1.0, 1.0, 2.0, 4.0, 8.0, 16.0, 32.0, 64.0, 128.0) × 10 mJy/beam. The restoring beam was a 0.05 mas (FWHM) circular Gaussian

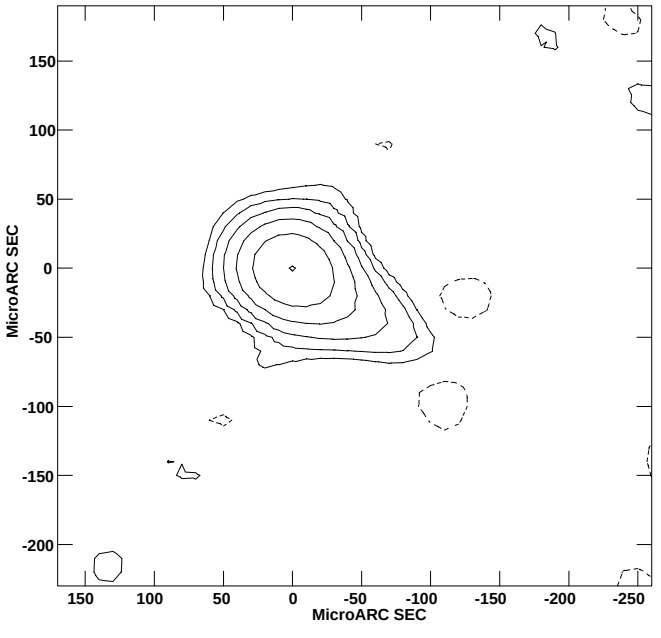

Fig. 14. BL Lac 100 GHz map from 1990 April 20. Peak flux density = 1.3 Jy/Beam. Contour intervals are chosen as (−4.0, 4.0, 8.0, 16.0, 32.0, 64.0, 128.0) × 10 mJy/beam. The restoring beam was a 0.05 mas (FWHM) circular Gaussian

Table 16. Model parameters for Gaussian components fitted to the 2145+067 UV data. Explanation of the parameters can be found in Table 5

	Year	Flux [Jy]	$\Delta\alpha$ [μas]	$\Delta\delta$ [μas]	Size [μas]
A	93	1.1 ± 0.2	-	-	<50

in PA ∼ 140° with a weak diffuse component at ∼10 mas in the same general PA. The core also appears to be embedded in a weak halo. VLA observations (Murphy et al. 1993) show a source with a second component ∼3 arcsec away in PA ∼ −45°, thus the extension seen at mas resolution is almost 180° away. This suggests that either the low frequency variability may affect the perceived structure or the jet twists dramatically as it moves out from the source.

This source has been detected at 215 GHz with an SNR of 124 on the baseline Pico Veleta – Plateau de Bure (Greve et al. 1995). Even at this high frequency it is therefore very bright and compact.

Our hybrid map shows a core weakly elongated in PA ∼ −120°. No significant structure is seen. The result of a Gaussian model fit to the *uv* data can be found in Table 16.

3.13. BL Lac

BL Lac exhibits very weak emission lines in the optical continuum above 5 Å (Stickel et al. 1993; Vermeulen et al. 1995). It is strongly variable at all wave-bands (Angel & Stockman 1980; Aller et al. 1985), and shows dramatic variations in polarization (Gagen-Thorn et al. 1994). VLBI observations at 10.7 GHz show a stationary core with components moving out with superluminal velocities in PA ∼ 190° (Mutel et al. 1990). Recent observations at λ18 cm (Bondi et al. 1996) show a single component extended in the NS direction. Previous maps by Bååth et al. (1992) showed an unresolved core with components moving out in PA ∼ −90° with a proper motion ≥90 μas/yr. The 3 mm 1988 epoch map convolved with a 0.5 mas circular Gaussian show a weak extended component at 1.5 mas in PA ∼ 200° agreeing with the structure seen at 10.7 GHz. Our map from 1990 April (Fig. 14) shows a core-jet structure with the jet in slightly different PA compared to the previous epoch at 100 GHz. This suggests that component E1 (Bååth et al. 1992) has moved in the general direction of the jet seen on larger scales. Most of the $\mathrm{Flux_{SD}}$ is seen on the shortest baselines (Table 2) suggesting that the emitted radiation at λ3 mm originates from the core. Some of the short baseline flux density has been lost in the mapping process. The result from model fitting Gaussian components to the *uv* data can be

Table 17. Model parameters for Gaussian components fitted to the BL Lac UV data. Explanation of the parameters can be found in Table 5

Year	Flux [Jy]	$\Delta\alpha$ [μas]	$\Delta\delta$ [μas]	Size [μas]	PA [°]
A 90	1.4 ± 0.2	-	-	<50	-
B 90	0.3 ± 0.1	-53 ± 6	-35 ± 6	50×10	-100 ± 24

found in Table 17. There is good agreement between the two methods. The extended jet seen in the image is very clear in the Gaussian model fit where it is represented by an elongated component.

The 1989 March map has a component $E1$ at $r \sim 90$ μas in PA $\sim -90°$. This component appears to have moved out and disappeared in our 1990 map. Assuming that component B has moved out from the core in the intervening time, then a lower limit to its proper motion is 63 ± 8 μas/year. This is a lower value than previously seen in this source (Bååth et al. 1992), but it is only a lower limit and may well be much higher.

3.14. 3C 446

The 100 GHz map on 3C 446 for the 1990 April epoch has been discussed extensively in Lerner et al. (1993). The map shows a central core with a component in PA $\sim -140°$ at a distance of 100 μas. The exact location of the component varied with the a priori models and the authors suggest that the map should be taken as a strong indication of a central core with a jet extending out from the core, rather than a full hybrid map of the source. The hybrid maps strongly suggest that the jet twists drastically going from μas to mas scales.

3.15. CTA 102

The arc-second scale structure of the source is dominated by a central core and two other components (Spencer et al. 1989). At λ18 cm the stronger component has a flux density of 0.2 Jy and is located at ∼1.6 arcsec in PA $\sim 140°$ while the weaker component is only 0.1 Jy at 1.0 arcsec in PA $\sim -40°$. Both components have a steep spectrum. Observations at λ6 cm (Wehrle & Cohen 1989), at λ18 cm, and at λ1.3 cm (Rantakyrö et al. 1996) show a central double knot feature (separated in NS direction by ∼3 mas) with an extended diffuse tail bending sharply to the SW. Rantakyrö et al. (1996), showed that the major contribution to the variability at wavelengths shorter than 32 cm is intrinsic to the source. Although we have only have one scan with closure phase information it was sufficient to make a rough hybrid map. The 1990 April map at 100 GHz (Fig. 15) resolves the northern component of the central double knot into two components. Due to the low declination of the source and the very poor UV-coverage the beam is very strongly elongated in the NS direction. We have chosen to present the image with the original beam since the convolved beam is markedly different from a circular Gaussian of 50 μas. The side lobe pattern results from the poor UV-coverage of the observations. The result from model fitting Gaussian components to the UV data can be found in Table 18.

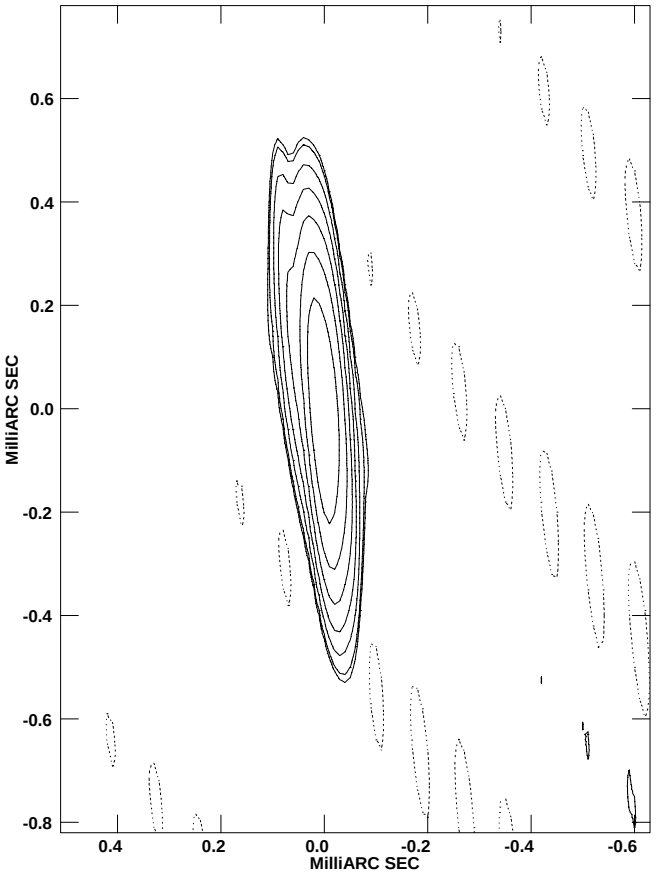

Fig. 15. CTA 102 100 GHz map from 1990 April 22. Peak flux density = 2.5 Jy/Beam. Contour intervals are chosen as (−3.0, 3.0, 4.0, 8.0, 16.0, 32.0, 64.0, 128.0) × 10 mJy/beam. The restoring beam was a elliptical Gaussian (0.44 × 0.03 mas in PA = 4.1°)

The model fit confirms the central structure with two strong components separated in an east west direction. We are unable to determine which of the components is the core, thus we cannot say how this structure is connected with the structure seen with mas resolution. It is clear that the jet twists and turns at it leaves the core. At λ3 mm the components appears to be separated in an EW direction while at λ1.3 cm the jet direction is NS and later the jet is shown to turn sharply to the E (Wehrle & Cohen 1989; Rantakyrö et al. 1996). Having only one

Table 18. Model parameters for Gaussian components fitted to the CTA 102 UV data. Explanation of the parameters can be found in Table 5. Since it is unclear what is the core in this image we give the position of the components relative to the phase center of the map. The large errors in δ are attributed to the heavily extended beam due to the very poor UV-coverage

	Year	Flux [Jy]	$\Delta\alpha$ [μas]	$\Delta\delta$ [μas]	Size [μas]
A	90	2.4 ± 2.4	80 ± 30	220 ± 300	<100
B	90	2.8 ± 2.2	3 ± 15	−50 ± 200	<100

epoch of observations with very limited UV-coverage we cannot say anything about the possible proper motion of components in this source; further observations are needed to investigate this.

3.16. 3C 454.3

This strong radio-source is an optically violent variable with high optical polarization. It is a strong γ-ray and X-ray source (Hartman et al. 1993). It has been observed extensively at lower resolutions (Pauliny-Toth et al. 1987) and at 43 GHz (Kemball et al. 1996). The mas structure is a typical core-jet structure with the extended jet in PA $\sim -65°$ (Padrielli et al. 1986). At λ7 mm the core is unresolved and there is a weaker component at PA $\sim 100°$ at 0.5 mas distance. λ3 mm VLBI observations made in 1993 and 1994 (Krichbaum et al. 1996a) show a central core with an extended jet in PA $\sim -70°$. Components in the jet are seen to be moving with $\beta_{\rm app} \sim 6-7$ c.

We found fringes only for one scan (6 min of data), not enough to make a hybrid map or a proper Gaussian model fit to the UV data. The baseline between Hat Creek and Kitt Peak had a flux density of ∼7 Jy.

4. Discussion

In the following discussion, it is assumed that the redshifts, z, are cosmological in origin with $H_0 = 100$ h km^{-1} Mpc^{-1} and $q_0 = 0.5$. The extended cosmological information on the sources can be found in Table 19.

We have presented the maps from the 1990 April and 1993 April observations of active galactic nuclei at λ3 mm with 50 μas resolution. These maps are among the highest resolution images of AGNs available to astronomers at this date and are vital to our understanding of the processes taking place in the central region of AGNs, especially the physical processesses behind the rapid structural changes. In spite of the limited dynamic range and long time between the epochs we are able to draw the following conclusions:

1. The core is very dominant at λ3 mm, any extended jet is in many cases resolved out or to weak compared with the core to be seen with our limited dynamic range. We can divide the observed sources into three groups:
   (a) Jet dominated: Our maps of sources that are dominated by a jet at lower frequencies (3C 84, 3C 273, and, 3C 279) or have an extended halo (2145+067) contain only a small fraction (less than 30%) of the single dish flux density. This is due to the effect that the interferometric array resolves out the large scale structures (i.e. jet or halo) that contain the major part of the flux density. We do not exclude the possibility that parts of the missing flux density also can be attributed to calibration and UV-coverage problems.
   (b) Core dominated sources: A few of the sources (0735+178, 1510−089, and BL Lac), typically those that are unresolved or have a simple structure with core and a single component close to the core, have all the single dish flux density present in the map. Most of their emission at λ3 mm is emitted from very compact (μas) components.
   (c) There are intermediate cases (1055+018, 3C 345, 3C 446, and OJ 287) where some flux density has been lost (∼50%) due to resolution effects, calibration inaccuracies, and the poor UV-coverage at short baselines.
2. It is clear from the maps that rapid structural changes take place.

Table 19. Cosmological information for the observed sources. z, is the measured redshift, r, is the linear size in cm corresponding to 10 μas at the distance of the source, v, is the velocity in units of c for a proper motion of 100 μas/year for a component, and μ, is the observed proper motion of this source from the 1990 and 1993 epochs

Source	z	r [cm]	v [c]	μ [μas/year]
3C 84	0.017	$7.4\ 10^{15}$	0.08	∼40/70/130
3C 111	0.049	$2.0\ 10^{16}$	0.22	-
0420−014	0.915	$1.3\ 10^{17}$	2.61	-
0735+178	0.424	$1.0\ 10^{17}$	1.53	-
0748+126	0.281	$8.1\ 10^{16}$	2.56	-
0748+126	0.889	$1.3\ 10^{17}$	2.56	-
OJ 287	0.306	$8.5\ 10^{16}$	1.18	>34
1055+018	0.888	$1.3\ 10^{17}$	2.56	-
3C 273B	0.158	$5.4\ 10^{16}$	0.67	-
3C 279	0.538	$1.1\ 10^{17}$	1.82	80 ± 10
1510−089	0.360	$9.3\ 10^{16}$	1.34	-
3C 345	0.593	$1.2\ 10^{17}$	1.96	-
2145+067	0.990	$1.3\ 10^{17}$	2.74	-
BL Lac	0.0686	$2.7\ 10^{16}$	0.31	63 ± 8
3C 446	1.404	$1.3\ 10^{17}$	3.34	∼100
CTA 102	1.037	$1.3\ 10^{17}$	2.82	-
3C 454.3	0.859	$1.3\ 10^{17}$	2.51	-

The process of determining proper motions of components from one epoch to another is fraught with several complications.

- In the cases where we have attempted to identify components then the difficulty of identification will function as a selection effect against high proper motions as the components with high proper motions will have moved too much to be unambigously identified.
- In some cases we are able to determine only lower limits to the proper motion, based on conservative assumptions of component motion. All this combined will give low values to the proper motions detected with the infrequent λ3 mm VLBI observations.

More frequent observations are needed to determine proper motions. We estimate that observations every month are required to obtain adequate time sampling to follow the ejection of components.

We see much lower proper motions at μas scales (Table 19) than the proper motions seen at mas scales (Table 3). It is important to state that this is not clear evidence for acceleration of components as they move out from the core, but rather a selection effect as discussed above.

3. The curvature and twisting of the jets seen at larger scales can also be seen at λ3 mm, but is even more pronounced (3C 84, OJ 287, 3C 345, BL Lac, CTA 102, and 3C 446). The PA of the components varies dramatically between μas and mas scales. The difference between μas and mas scale jet, ΔPA, is in these cases $\sim$90°. Some sources, on the other hand, exhibit jets that are straight from μas to mas scales, i.e. 3C 111, 0735+178, 0748+126, 1055+018, 3C 273, and 3C 279. This modality in ΔPA has been observed previously looking at the difference in PA between VLBI and VLA images (Pearson & Readhead 1988; Wehrle et al. 1992). Conway & Murphy (1993) explained this modality by having two different populations of AGNs. The misaligned population has parsec scale jets in the form of low pitch helices and the aligned population has straight jets with small changes in PA due to intrinsic bends. The modality seen in ΔPA between mmVLBI and on VLBI then implies that the curvature in the helical jets increases as we get closer to the core. Note all the misaligned sources are either core dominated (point 1.b above) or intermediate cases (point 1.c above) strengthening the case for applying the Conway & Murphy model to our λ3 mm VLBI observations, and the grouping of objects into two groups does not address which actual physical process causes the observed helicity.
4. The majority of the sources exhibit an unresolved core even with 50μas resolution. The diameters of the core seen in our maps range from $10^{16} - 10^{17}$ cm, still magnitudes larger than the expected Schwarzschild radius of the MBH, $R_s = 10^{13} - 10^{14}$ cm (Band & Malkan 1989), but close to the expected size of the accretion disc or torus, $40 \times R_s$.

With λ3 mm VLBI a intricate picture of the inner regions of AGN's emerges. Our unique observations show some sources with components moving along twisted paths, other sources where components move along a straight jet from μas to mas scales, weak superluminal motion, and tentative support for acceleration (although the last feature may be a selection effect as discussed above).

One model proposed to explain the helical structure seen in many sources is the helical jet model proposed by Hardee (1987). In this model the observed components are interference points of Kelvin-Helmholtz instabilities traveling down a conical, adiabatically expanding flow. Numerical simulations of slabs propagating down such a flow (Hardee et al. 1992) show that the jet can remain collimated over large distances, before the oscillations become large enough to disrupt it. The simulations also show that the oscillation wavelength could scale with the distance from the core.

Another model which also has been successful in modeling the helical structure of 3C 345 (Steffen et al. 1995) is the jet model by Camenzind & Krockenberger (1992). This model uses bulk relativistic plasma moving along helical magnetic field lines, driven by magnetized accretion disc winds.

Our data are not of sufficient quality to discern which of these two main models is best suited to explain the observed helicity.

The ΔPA observed by us strongly suggests that any model trying to explain the appearance of the jets of the misaligned jet population, needs to scale with distance from the core, thus models that are scale-free face severe problems.

We conclude that λ3 mm VLBI is a very promising tool for investigating the central regions of AGN's. Our observations are limited by dynamic range and the long time between epochs but we have newer epochs in the process of being reduced that will improve both of these weak points.

Acknowledgements. We would like to thank the people at the individual telescopes for helping in making the observations, without their support these observations would not have been possible. We would also like to thank the people at the Haystack correlator for their help in correlating these experiments. Without the help of D. Graham and A. Greve VLBI observations at Pico Veleta would not have been possible. We further would like to thank K. Standke for his help with the observation and calibration.

Fredrik T. Rantakyrö acknowledges support for his research by the European Union under contract ERBCHGECT920011. Part of this research was carried out at the Onsala Space Observatory. Onsala Space Observatory at Chalmers University of Technology is the Swedish National Facility for Radio Astronomy. The Hat Creek array is operated

by the Berkeley-Illinois-Maryland Association with funding from the National Science Foundation, Grant AST 93-20238 to the University of California. The NRAO is a facility of the National Science foundation, operated under cooperative agreement by Associated Universities, Incorporated. FCRAO is operated with support of the National Science Foundation under grant AST 91-15721 and with permission of the Metropolitan District Commission of the Commonwealth of Massachusetts. This is contribution number 819 of the Five College Astronomy Department. The work of T.P.K. was supported in part by the German Verbundforschung. The hydrogen maser and the VLBA terminal at Pico Veleta were financed by the Stiftung Volkswagenwerk. This research has made use of the NASA/IPAC Extra-galactic database (NED), which is operated by the Jet Propulsion Laboratory, Caltech, under contract with the National Aeronautics and Space Administration.

References

Alberdi A., Krichbaum T.P., Graham D.A., et al., 1997, A&A 327, 513
Aller H.D., Aller M.F., Latimer G.E., Hodge P.E., 1985, ApJS 59, 513
Angel J.R.P., Stockman H.S., 1980, ARA&A 18, 321
Band D.L., Malkan M.A., 1989, ApJ 345, 122
Biretta J.A., Moore R.L., Cohen M.H., 1986, ApJ 308, 93
Bondi M., Padrielli L., Fanti R., et al., 1996, A&A 308, 415
Bregman J.N., Glassgold A.E., Huggins P.J., et al., 1986, ApJ 301, 708, 1986
Bååth L.B., Padin S., Woody D., et al., 1991, A&A 241, L1
Bååth L.B., Zhang, 1991, A&A 1991, 243, 328
Bååth L.B., Rogers A.E.E., Inoue M., et al., 1992, A&A 257, 31
Camenzind M., Krockenberger M., 1992, A&A 255, 59
Carrara E.A., Abraham Z., Unwin S.C., Zensus J.A., 1993, A&A 279, 83
Chiang J., Fichtel C.E., Von Montigny C., Nolan P.L., Petrosian V., 1995, ApJ 452, 156
Conway J.E., Murphy D.W., 1993, ApJ 411, 89
Cotton W.D., 1979, ApJ 229, L115
Courvoisier T.J.-L., Robson E.I., Blecha A., et al., 1988, Nat 335, 330
Davis R.J., Muxlow T.W.B., Conway R.G., 1985, Nat 318, 343
Della Ceca R., Palumbo G.G.C., Persic M., et al., 1990, ApJS 72, 471
de Pater I., Perley R.A., 1983, ApJ 273, 64
Gabuzda D.C, Wardle J.F.C., Roberts D.H., 1989, ApJ 336, L59
Gabuzda D.C., Mullan C.M., Cawthorne T.V., Wardle J.F.C., Roberts D.H., 1994, ApJ 435, 128
Gagen-Thorn V.A., Marchenko S.G., Yurchenko A.V., Yakoleva V.A., 1994, AR 38, 635
Gregorini L., Mantovani F., Eckart A., et al., 1984, AJ 89, 323
Greve A., Torres M., Wink J.E., et al., 1995, A&A 299, L33
Hardee P.E., 1987, ApJ 318, 78
Hardee P.E., White R.E., Norman M.L., Cooper M.A., Clarke D.A., 1992, ApJ 387, 460
Hartman R.C., Bertsch D.L., Dingus B.L., et al., 1993, ApJ 407, L41
Kemball A.J., Diamond P.J., Pauliny-Toth I.I.K., 1996, ApJ 464, L55
Krichbaum T.P., Britzen S., Standke K.J., et al., 1996a, in: Quasars and Active Galactic Nuclei: High Resolution Radio Imaging, Cohen M.H. and Kellermann K.I. (eds.) PNAS, U.S.A., Vol. 92, No. 5, p. 11377
Krichbaum T.P., Witzel A., Graham D., Lobanov A.P., 1996b, in: MM-VLBI Science Workshop, Barvainis R. & Phillips R.B. (eds.) Haystack MIT Cambridge, p. 3
Krichbaum T.P., Standke K.J., Witzel A., et al., 1994a, in: Proceedings of the 2nd EVN/JIVE Symposium, Kus A.J., Schilizzi R.T., Borkowski K.M. and Gurvits L. (eds.), Torun Radio Astronomy Observatory. Nicolaus Copernicus University, Torun, Poland, p. 47
Krichbaum T.P., Standke K.J., Graham D.A., et al., 1994b, in: Multi-Wavelength Continuum Emission of AGN, IAU Symp. 159, Courvoisier T.J.-L. & Blecha A. (eds.). Kluwer, Dordrecht, p. 187
Krichbaum T.P., Witzel A., Graham D.A., et al., 1993, A&A 275, 375
Krichbaum T.P., Witzel A., Graham D.A., et al., 1992, A&A 260, 33
Krichbaum T.P., Booth R.S., Kus A.J., et al., 1990, A&A 237, 3
Ku H.-M., Helfland D.J., Lucy L.B., 1980, Nat 288, 323
Lainela, et al., 1993, in: Variability in Blazars, Valtaoja E. & Valtonen M. (eds.). Cambridge University Press, Cambridge, p. 102
Leppänen K.J., Zensus J.A., 1995, ApJ 110, 2479
Lerner M.S., Bååth L.B., Inoue M., et al., 1993, 280 A&A 117
Lin Y.C., Bertsch D.L., Dingus B.L., et al., 1993, ApJ 416, L53
Litchfield S.J., Stevens J.A., Robson E.I., Gear W.K., 1995, MNRAS 274, 221
Maraschi L., Grandi P., Urry M., et al., 1994, ApJ 435, L91
Marscher A.P., Gear W., 1985, ApJ 421, 153
Marscher A.P., Gear W., Travis, 1993, in: Variability in Blazars, Valtaoja E. & Valtonen M. (eds.). Cambridge University Press, Cambridge, p. 85
Montigny Von C., Bertsch D.L., Chiang J., et al., 1995, ApJ 440, 525
Moore R.L., Readhead A.C.S., Bååth L.B., 1983, Nat 306, 44
Murphy D.W., Brown I.W.A., Perley R.A., 1993, MNRAS 264, 298
Mutel R.L., Phillips R.B., Bumei S., Bucciferro R.R., 1990, ApJ 352, 81
Padrielli L., Romney J.D., Bartel N., et al., 1986, A&A 165, 53
Pauliny-Toth I.I.K., Porcas R.W., Zensus J.A., et al., 1987, Nat 328, 778
Pearson T.J., Readhead A.C.S., 1988, ApJ 328, 114
Preuss E., Alef W., Shengyin W., et al., 1990, in: Parsec scale jets, Zensus J.A. & Pearson T.J. (eds.). Cambridge University Press, Cambridge, p. 120
Radecke H.D., Bertsch D.L., Dingus B.L., et al., 1995, ApJ 438, 659
Rantakyrö F.T., Bååth L.B., Dallacasa D., Jones D.L., Wehrle A.E., 1996, A&A 310, 66
Roberts D.H., Gabuzda D.C., Wardle J.F.C., 1987, ApJ 323, 536
Schalinski C.J., Witzel A., Krichbaum T.P., et al., 1994, in: Compact Extragalactic Radio Sources, Zensus J.A. & Kellermann K.I. (eds.). NRAO, Socorro, p. 45

Spencer R.E., McDowell J.C., Charlesworth M., et al., 1989, MNRAS 240, 657
Standke K.J., Graham D.A., Krichbaum T.P., et al., 1994, in: VLBI Technology, Progress and Future Observational Possibilities, Sasao T., Manabe S., Kameya O. and Inoue M. (eds.). Terra Scientific Publishing Company, Tokyo, p. 75
Steffen W., Zensus J.A., Krichbaum T.P., Witzel A., Qian S.J., 1993, A&A 302, 335
Steffen W., Krichbaum T.P., Witzel A., 1993, in: Sub-arc-second Radio Astronomy, Davis R.J. & Booth R.S. (eds.). Cambridge University Press, Cambridge, p. 363
Stevens J.A., Litchfield S.J., Robson E.I., et al., 1996, ApJ 466, 158
Stickel M., Fried J.W., Kuhr H., 1993, A&AS 98, 393
Takalo L.O., 1994, IAU159, Courvoisier T.J.-L. & Blecha A. (eds.). Kluwer, Dordrecht, p. 409
Tateyama C.E., Inoue M., Krichbaum T.P., et al., 1996, PASJ 48, 37
Tornikoski M., Valtaoja E., Terasranta H., et al., 1996, A&AS 116, 157
Unwin S.C., Cohen M.H., Pearson T.J., Seielstad G.A., Simon R.S., 1983, ApJ 271, 536
Unwin S.C., Cohen M.H., Biretta J.A., Hodges M.W., Zensus J.A., 1989, ApJ 340, 117
Unwin S.C., 1990, in: Parsec Scale Jets, Zensus J.A. & Pearson T.J. (eds.). Cambridge University Press, Cambridge, p. 93
Venturi T., Readhead A.C.S., Marr J.M., et al., 1993, ApJ 411, 552
Vermeulen R.C., Cohen M.H., 1994, ApJ 430, 467
Vermeulen R.C., Ogle P.M., Tran H.D., et al., 1995, ApJ 452, L5
Wehrle A.E., Cohen M.H., 1989, ApJ 346, L69
Wehrle A.E., Cohen M.H., Unwin S.C., et al., 1992, ApJ 391, 589
Whitney A.R., Shapiro I.I., Rogers A.E.E., et al., 1971, Sci 173, 225
Wills D., Wills B.J., 1976, ApJS 31, 143
Wills B.J., Wills D., Breger M., et al., 1992, ApJ 398, 454
Wright M.C.H., Backer D.C., Carlstrom J.E., et al., 1988, ApJ 329, L61
Zensus, 1987, in: Superluminal Radio Sources, Zensus J.A. & Pearson T.J. (eds.). Cambridge University Press, Cambridge, p. 11
Zensus J.A., Unwin S.C., Cohen M.H., et al., 1990, AJ 100, 1777
Zensus J.A., Cohen M.H., Unwin S.C., 1995, ApJ 443, 35